Biochemistry

Article

Cite This: Biochemistry 2018, 57, 3713−3721

pubs.acs.org/biochemistry

Steric Control of the Rate-Limiting Step of UDP-Galactopyranose Mutase

Gustavo Pierdominici-Sottile,[†] Rodrigo Cossio-Pérez,[†] Isabel Da Fonseca,[‡] Karina Kizjakina,[‡] John J. Tanner,[*,§] and Pablo Sobrado[*,‡]

[†]Sci-prot. Departamento de Ciencia y Tecnología, Universidad Nacional de Quilmes, Bernal B1876BXD, Argentina

[‡]Department of Biochemistry, Virginia Tech, Blacksburg, Virginia 24061, United States

[§]Departments of Biochemistry and Chemistry, University of Missouri—Columbia, Columbia, Missouri 65211, United States

Supporting Information

ABSTRACT: Galactose is an abundant monosaccharide found exclusively in mammals as galactopyranose (Gal*p*), the six-membered ring form of this sugar. In contrast, galactose appears in many pathogenic microorganisms as the five-membered ring form, galactofuranose (Gal*f*). Gal*f* biosynthesis begins with the conversion of UDP-Gal*p* to UDP-Gal*f* catalyzed by the flavoenzyme UDP-galactopyranose mutase (UGM). Because UGM is essential for the survival and proliferation of several pathogens, there is interest in understanding the catalytic mechanism to aid inhibitor development. Herein, we have used kinetic measurements and molecular dynamics simulations to explore the features of UGM that control the rate-limiting step (RLS). We show that UGM from the pathogenic fungus *Aspergillus fumigatus* also catalyzes the isomerization of UDP-arabinopyranose (UDP-Ara*p*), which differs from UDP-Gal*p* by lacking a -CH_2-OH substituent at the C5 position of the hexose ring. Unexpectedly, the RLS changed from a chemical step for the natural substrate to product release with UDP-Ara*p*. This result implicated residues that contact the -CH_2-OH of UDP-Gal*p* in controlling the mechanistic path. The mutation of one of these residues, Trp315, to Ala changed the RLS of the natural substrate to product release, similar to the wild-type enzyme with UDP-Ara*p*. Molecular dynamics simulations suggest that steric complementarity in the Michaelis complex is responsible for this distinct behavior. These results provide new insight into the UGM mechanism and, more generally, how steric factors in the enzyme active site control the free energy barriers along the reaction path.

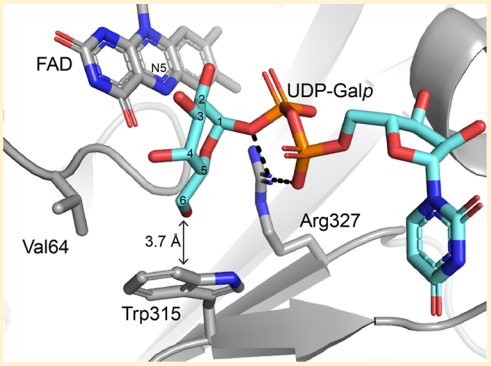

Galactofuranose (Gal*f*) is an important structural component of the cell wall of fungi and mycobacteria and is a cell surface virulence factor in several parasitic human pathogens.[1−3] Gal*f* biosynthesis starts with the isomerization of UDP-galactopyranose (UDP-Gal*p*) to UDP-galactofuranose (UDP-Gal*f*), which is catalyzed by UDP-galactopyranose mutase (UGM) (Scheme 1A).[4,5] UGM is a flavin-dependent enzyme that requires the reduced form of FAD for activity, despite the reaction being redox neutral.

Extensive mechanistic and structural studies have provided a clear description of galactose isomerization catalyzed by UGM (Scheme 2).[6−10] The initial stage involves the reaction of the oxidized flavin with NAD(P)H yielding the reduced form of the enzyme, which is required for activity.[11] The reduced flavin, acting as a nucleophile, attacks the anomeric carbon atom of Gal*p*, yielding a flavin−galactose adduct and breaking the glycosidic bond to UDP. After the covalent adduct is formed, the sugar ring is opened, leading to formation of a FAD−iminium intermediate. Next, the ring closure step forms Gal*f*. Ring closure is considered to be the rate-limiting step (RLS) of the mechanism.[7] Lastly, the catalytic cycle is completed when the flavin−Gal*f* adduct breaks and the glycosidic bond is reestablished, yielding the final UDP-Gal*f* product.[6−10]

Crystal structures have provided support for several of the steps in the mechanism. The structural basis for enzyme cofactor reduction is known from the structures of oxidized *Aspergillus fumigatus* UGM (*Af*UGM) complexed with NAD(P)H.[12] The structure of the E−S Michaelis complex is known for several UGMs, including *Af*UGM,[13,14] another eukaryotic UGM from *Trypanosoma cruzi* (*Tc*UGM),[15] and bacterial UGMs.[16−24] Furthermore, the flavin−galactose adduct has been trapped *in crystallo*, providing direct structural evidence of flavin functioning as a nucleophile.[25] These and other structures have also revealed large conformational changes associated with reduction of the cofactor and substrate binding.[26]

Herein, we explore the features of the active site that control the RLS of UGM. Using kinetic solvent isotope effects (KSIEs), kinetic solvent viscosity experiments (KSVEs), and rapid reaction kinetic analyses, we show that the RLS of *Af*UGM changes from ring contraction to product release when using the non-natural substrate UDP-arabinofuranose (UDP-Ara*f*).

Received: March 16, 2018
Revised: May 9, 2018
Published: May 14, 2018

DOI: 10.1021/acs.biochem.8b00323
Biochemistry 2018, 57, 3713−3721

Scheme 1. Reactions Catalyzed by UDP-Galactopyranose Mutase (UGM), (A) the Reaction of UGM with the Natural Substrate UDP-Galactopyranose (UDP-Gal*p*) and (B) the Reaction of UGM with the Non-Natural Substrate UDP-Arabinopyranose (UDP-Ara*p*)[a]

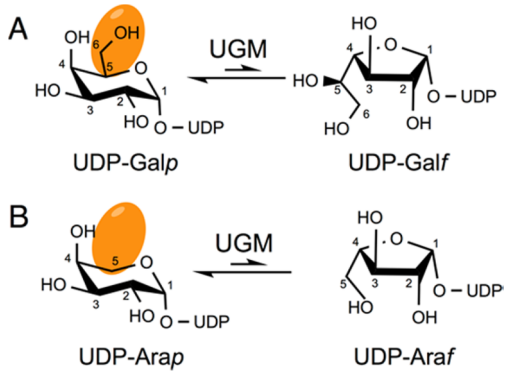

[a]The difference between the two substrates is highlighted in orange.

This finding suggested that residues near the C6 hydroxyl of UDP-Gal*p*/*f* are important for fast product release. Previous crystal structures of *Af*UGM show that Trp315 is uniquely positioned to play this role. Mutation of Trp315 to Ala in the *Af*UGM variant W315A switched the RLS with UDP-Gal*f* to product release, mimicking the kinetic signature of the wild-type enzyme with UDP-Ara*f*. To investigate the process at the atomic level, we also performed classical molecular dynamics (MD) simulations to characterize the Michaelis complex and quantum-classical MD simulations to study the chemical steps of the mechanism. The computational analysis shows that furanose ring formation is the RLS with UDP-Gal*p*, because of restricted rotation of the hydroxyl groups in the compact space imposed in part by Trp315. In contrast, with UDP-Ara*p*, the lack of the -CH_2-OH group decreases the size of the physical constraints in the active site, lowering the activation energy for recyclation. Altogether, these results provide new insight into the UGM mechanism and show how steric factors in the enzyme active site control the free energy barriers along the reaction path.

EXPERIMENTAL DETAILS

Materials. UDP and UDP-Gal*p* were acquired from Sigma, and UDP-Ara*f* was acquired from the Complex Carbohydrate Research Center (University of Georgia, Athens, GA). *Pfu*Ultra hotstart high-fidelity DNA polymerase was obtained from Agilent Technologies (Santa Clara, CA). DpnI was purchased from Fisher Scientific (Hampton, NH). *Escherichia coli* TOP-10 chemically competent cells were obtained from Invitrogen (Carlsbad, CA). *E. coli* BL21 (DE3) chemically competent cells were obtained from Promega (Madison, WI). The plasmid miniprep kit was from Qiagen (Valencia, CA). Primers were from IDT Integrated DNA Technology (Coralville, IA). All other buffers and chemicals were purchased from Fisher Scientific.

Scheme 2. Detailed Mechanism for the Reaction Catalyzed by Wild-Type *Af*UGM with the Natural Substrate UDP-Gal*p*[a]

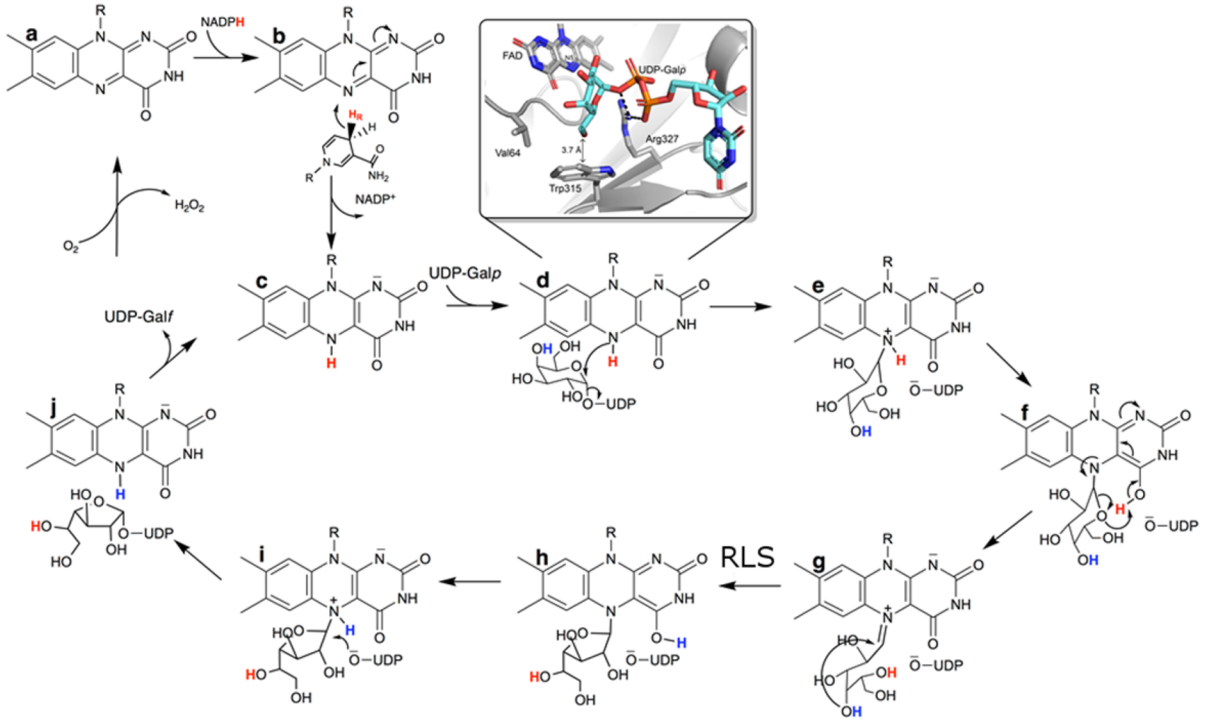

[a]Red color denotes the H atom initially bonded to $N5_{FADH}$ and subsequently transferred as a proton to the substrate. Steps a → b and b → c involve the FAD reduction by NADPH. Once FAD is reduced, the substrate (UDP-Gal*p*) enters the active site (c → d). A covalent adduct is formed between the substrate and the FADH cofactor (d → e), temporarily breaking the glycosidic bond, followed by an internal proton transfer between $N5_{FADH}$ and $O6_{FADH}$ (e → f). Step f → g involves linearization of the sugar and formation of the iminium ion species. In the next step (g → h), the sugar cyclizes into its five-membered ring form. This step is isotope sensitive and is considered to be the chemical rate-limiting step (RLS) of the mechanism.[7] Once the furanose form of the sugar is reached, another internal proton transfer takes place (h → i), and the glycosidic bond to UDP is formed (i → j). Finally, the product of the reaction exits the active site of the enzyme.

DOI: 10.1021/acs.biochem.8b00323
Biochemistry 2018, 57, 3713−3721

Site-Directed Mutagenesis. Primers of 25 bp were designed to insert a point mutation to create the *A. fumigatus* W315A mutant (W315A). Site-directed mutagenesis was performed using the QuikChange site-directed mutagenesis kit following instructions provided by the manufacturer. The UGM gene cloned into pVP55A was used as the DNA template.[13] The mutation was confirmed by DNA sequencing.

Expression and Purification. Wild-type UGM and mutant UGM from *A. fumigatus* were expressed in autoinduction medium as a fusion to His_8 tags and purified following protocols previously reported.[7,11,13,15] In general, 0.6 mg of purified protein was obtained per gram of bacterial cell paste.

Kinetic Characterization. The enzymatic activity for recombinant UGM was determined by monitoring the formation of UDP-Gal*p* or UDP-Ara*p* from UDP-Gal*f* or UDP-Ara*f* on a high-performance liquid chromatography (HPLC) instrument. The assay was performed as described previously by Oppenheimer et al.[7] The assays were performed in 25 mM HEPES, 125 mM NaCl, and 20 mM dithionite (to reduce the flavin and make the solution temporarily anaerobic), at pH 7. The enzyme concentration was determined on the basis of the flavin bound to UGM using an extinction coefficient at 450 nm (ε_{450}) of 10.6 mM^{-1} cm^{-1}. The reaction was initiated by addition of 30 nM *Af*UGM or 1 μM W315A. The reaction mixture for *Af*UGM was incubated at 37 °C for 1 min, and the mutant was incubated for 5 min. The reaction was stopped by heat denaturation and the denatured protein pelleted by centrifugation. The supernatant was injected onto a Dionex CarboPac PA100 column. UDP-Gal*p* and UDP-Gal*f* were eluted isocratically with 75 mM KH_2PO_4 (pH 4.5) at a rate of 0.80 mL/min and monitored at 262 nm. Under these conditions, UDP-Gal*p* eluted at 27.4 min, UDP-Gal*f* at 34.2 min, UDP-Ara*p* at 30.3 min, and UDP-Ara*f* at 41.1 min. The conversion was quantified by the percentage of the substrate and product peaks. Kinetic parameters were determined by fitting the initial velocity data to the Michaelis–Menten equation.

Kinetic Solvent Viscosity Effects. To determine whether product release limits the rate of the reaction, viscosity effects were measured for *Af*UGM and W315A. Reactions were performed as described above with 1000 μM UDP-Gal*f* or UDP-Ara*f* in the presence of 0, 5, 10, 20, and 30% glycerol. The relative viscosity (η_{REL}) of the reaction was calculated using a reference table for different percentages of glycerol in solution.[27]

Kinetic Solvent Isotope Effects. To determine the solvent kinetic isotope effect for *Af*UGM and W315A, initial velocities were measured at various concentrations of UDP-Gal*f* or UDP-Ara*f* in either H_2O or 90% D_2O at pD 7.0 as previously reported.[7] The enzymatic activity was determined as described above.

Monitoring the Reaction of Reduced Flavin with UDP-Ara*f*. The assay was performed in the stopped-flow spectrophotometer under anaerobic conditions. Removal of oxygen from the stopped-flow system was achieved through addition of a solution of 100 mM glucose with 0.1 mg/mL glucose oxidase from *Aspergillus niger* in 0.1 M sodium acetate (pH 5.0) overnight. Sodium phosphate at 50 mM (pH 7.0) was degassed by five cycles of vacuum and argon flushing, each for 30 min. The enzyme solution was made anaerobic by degassing with six cycles of vacuum for 15 min and flushing with anaerobic argon between cycles. UDP and UDP-Ara*f* were solubilized in degassed buffer, and concentrations were verified by a spectrophotometer at 262 nm. To reduce the degassed *Af*UGM, 20 mM sodium dithionite was added to the enzyme and the excess dithionite was removed using a desalting column. Reduced UGM at a final concentration of 20 μM was mixed with a final concentration of 0.25 mM UDP-Ara*f* or 0.25 mM UDP. Spectra were collected on a logarithmic time base from 1 ms to 30 s using a photodiode array spectrophotometer.

Initial MD Settings and Equilibration Protocol. The crystal structure of reduced *Af*UGM complexed with UDP-Gal*p* (PDB entry 3UTH) was used to generate the initial coordinates of the *Af*UGM/UDP-Gal*p* simulation. Gal*p* was replaced with Ara*p* to create the initial coordinates for the *Af*UGM/UDP-Ara*p* simulation. This assumes that the introduced modification of the substrate does not significantly alter the structure of the enzyme–substrate system and that misleading conformations will be corrected during the simulation. Standard protonation states were assigned to all the residues except for His62, which was protonated according to experimental results.[15] The structures were solvated in a 12 Å periodic truncated octahedral cell of TIP3P water molecules, and counterions were used for charge neutralization. The Amber99SB force field was used to compute the potential energy of the protein. The FADH cofactor and substrates UDP-Gal*p* and UDP-Ara*p* were parametrized as described previously.[28] Systems were minimized at a constant volume and then heated to 303 K during 500 ps using the weak-coupling algorithm with a τ_{tp} value of 3.5 ps. This was followed by a 500 ps period of equilibration under constant-temperature and -pressure conditions at 303 K and 1 bar using 3.5 ps for both τ_{tp} and τ_p. The electrostatic cutoff was set to 10 Å. We monitored the temperature and density of the system until they reached plateaus. The obtained structure was used as the starting point for classical and quantum-classical molecular-mechanics (QMMM) simulations.

Classical MD Simulations. From the equilibrated structures, we performed 10 equivalent classical MD simulations for each Michaelis complex: *Af*UGM/UDP-Gal*p* and *Af*UGM/UDP-Ara*p*. In each case, the trajectories were started considering distinct initial atomic velocities, which were randomly chosen from a Maxwellian distribution at 303 K. The production phases lasted 100 ns, and snapshots of the trajectories were collected every 0.5 ns. Data corresponding to the distributions presented were computed considering the whole group of trajectories, while temporal evolution of the distances corresponds to individual trajectories that are representative of the behavior of the whole group of simulations.

QMMM MD Simulations. QMMM MD simulations were performed considering the QM subsystem constituted by the flavin cofactor, the substrate (either UDP-Gal*p* or UDP-Ara*p*), Gly62, His63, and the side chains of Arg91, Arg182, Arg327, and Arg447. The self-consistent charge density functional tight binding (scc-DFTB) method was implemented to describe the potential energy of this subsystem. This method has proven itself to be suitable for describing the energetics of chemical and biochemical reactions.[29−31] It has also been shown to provide the best semiempirical description for six-member carbohydrate ring deformation.[32] Starting from the corresponding Michaelis complex of each system (*Af*UGM/UDP-Gal*p* or *Af*UGM/UDP-Ara*p*), we employed the umbrella sampling technique to investigate each chemical step of the catalytic mechanism. In Figure S1, we present a detailed representation of how each reaction coordinate was defined for each step of the

DOI: 10.1021/acs.biochem.8b00323
Biochemistry 2018, 57, 3713−3721

mechanism. For the sake of completeness, we will briefly describe the procedure here, placing a specific emphasis on the ring closure step because it is considered the rate-limiting one. The first chemical step of the catalytic mechanism involves the formation of the flavin−Arap/Galp adduct (step d → e in Scheme 2 and step 1 in Figure S1). Then, an internal proton transfer between $N5_{FADH}$ and $O4_{FADH}$ occurs (step e → f in Scheme 2 and step 2 in Figure S1) prior to the ring opening process (step f → g in Scheme 2 and step 3 in Figure S1). At this stage, the sugar reaches a linear form. The next step involves cyclization of the sugar into a five-member ring form. This process has been implicated in the rate determinant step for the Galp−Galf conversion by both theoretical and experimental studies[7,28,33] and is sensitive to the solvent isotopic kinetic effect. In this step of the catalytic mechanism, $O4_{GAL/ARA}$ transfers a hydrogen atom to $O4_{FADH}$ and forms a new bond with the anomeric sugar carbon ($C1_{GAL/ARA}$), producing closure of the ring into its five-membered form (step g → h in Scheme 2 and step 4 in Figure S1). To sample the configurations from this process, we defined the reaction coordinate (ε_4) using a linear combination of three distances related to the atoms involved in the reaction. In particular, $\varepsilon_4 = d_8 - d_9 - d_{10}$, where d_8, d_9, and d_{10} represent the distances between $O4_{GAL/ARA}$ and H, H and $O4_{FADH}$, and $O4_{GAL/ARA}$ and $C1_{GAL/ARA}$, respectively. Reaction coordinate ε_4 was sampled from −5.00 to −0.48 Å considering 0.08 Å wide windows. Harmonic restraints of 225.0 kcal mol^{-1} $Å^{-2}$ were applied to force the system to wander around the selected values of the reaction coordinate. Within each window, an equilibration phase of 50 ps was followed by a production phase of 0.2 ns. The actual values of the reaction coordinate were recorded every 2 fs. The last 30000 values of each window were used to compute the unbiased probability by means of the weighted histogram analysis method (WHAM).[34] The DHAM methodology was also implemented as a way to check the consistency of the results.[35] When following each reaction coordinate, the last structure of a given window was used as the starting point for the next window.

To further check the convergence of the free energy computations, we performed other tests. First, we compared the free energy profiles obtained using the first half of the data (i.e., the first 15000 values selected at each specific value of the reaction coordinate) with those obtained using the second half. The reaction coordinate was sampled both forward and backward. Finally, we repeated the reaction path three times starting from a different initial configuration. The average values for the barrier of this reaction and the standard deviation were computed considering six distinct but equivalent paths, formed by each forward and backward path from each of the three independent calculations.

The same protocol, except for the triple repetition of the independent simulations, was implemented for every step of the catalytic mechanism. The distances involved in the definition of each reaction coordinate are depicted in Figure S1. These are the same as the ones employed by us to study the Galp−Galf conversion in the catalytic mechanism of *Tc*UGM.[28] When each reaction intermediate was reached, simulations of 0.5 ns without any restraint were performed to check their stability.

RESULTS

***Af*UGM Catalyzes the Interconversion of UDP-Arap/f.** UDP-Araf has been shown to be a substrate for bacterial UGM; however, to the best of our knowledge, it has not been evaluated with any eukaryotic UGM.[36] As a baseline for this analysis, the kinetic parameters of wild-type *Af*UGM with the natural substrate were first determined. Activity was measured by monitoring the amount of UDP-Galp formed at various concentrations of UDP-Galf. The protein was reduced with excess dithionite and the product separated and analyzed using the HPLC assay described in Experimental Details. The initial rates exhibited Michaelis−Menten behavior (Figure 1A). Fitting of the data yielded a k_{cat} of 100 s^{-1} and a K_M of 450 μM (Table 1).

The activity of *Af*UGM with UDP-Araf was determined as described for UDP-Galf (Figure 1B). The k_{cat} value with UDP-Araf was ∼700-fold lower than for UDP-Galf, while the K_M value was ∼5-fold lower, which resulted in a 150-fold decrease in k_{cat}/K_M. Thus, *Af*UGM catalyzes UDP-Arap/f conversion, albeit with a catalytic efficiency much lower than that of the natural substrate.

***Af*UGM Forms an Iminium Intermediate with UDP-Araf.** The flavin−sugar iminium ion is a hallmark of the UGM reaction mechanism (Scheme 2, species g), so we asked whether such a species is formed with UDP-Araf. Changes in the absorbance spectrum of reduced *Af*UGM were monitored in the stopped-flow spectrophotometer under anaerobic conditions. The enzyme was initially mixed with buffer alone, and no absorbance changes were observed (data not shown).

Similarly, the spectra remained unchanged when UDP was added (Figure S2A). In contrast, when UDP-Araf was introduced, a decrease in absorbance at ∼450 nm and an increase at ∼380 nm were detected (Figure S2B). These absorbance changes are consistent with those previously reported by us and others for iminium ion formation in UDP-Galp/f isomerization catalyzed by UGMs.[7,8] These results suggest that the *Af*UGM-catalyzed isomerization of UDP-Arap to UDP-Araf also proceeds via an iminium ion intermediate.

The *Af*UGM W315A Variant Is Kinetically Compromised. We sought a structural explanation for the low activity of *Af*UGM with UDP-Araf. The only difference between UDP-Arap and UDP-Galp is the presence of a -CH_2-OH group at position C5 of the latter substrate (Scheme 1). The crystal structure of *Af*UGM complexed with UDP-Galp shows that this group packs tightly against Trp315 (Scheme 2d, inset). This residue is highly conserved in eukaryotic UGMs. Sequence alignment shows that it is conserved in 114 of 124 sequences analyzed (Figure S3).

W315A was purified following the procedure developed for *Af*UGM. The protein contained tightly bound FAD and upon reduction was able to catalyze UDP-Galp/f isomerization; however, the activity was much lower than that of wild-type *Af*UGM. The k_{cat} and k_{cat}/K_M values of W315A were 160−370-fold lower than those of the wild type, while the K_M value changed by ∼2-fold (Table 1 and Figure 1C). In summary, the kinetic parameters of W315A with the natural substrate are similar to those of wild-type *Af*UGM with UDP-Araf. The activity of W315A with UDP-Araf was also determined. Compared with those of *Af*UGM, the k_{cat} and K_M values were 1.6- and ∼7-fold higher, respectively. These changes resulted in a modest ∼5-fold decrease in k_{cat}/K_M (Table 1).

Kinetic Solvent Isotope Effects. To investigate if a chemical step in the reaction is rate-limiting, we measured the KSIE. In KSIE experiments, H_2O is replaced by D_2O, allowing the exchange of ionizable protons. The rate measured under these conditions should decrease if proton transfer takes place

DOI: 10.1021/acs.biochem.8b00323
Biochemistry 2018, 57, 3713−3721

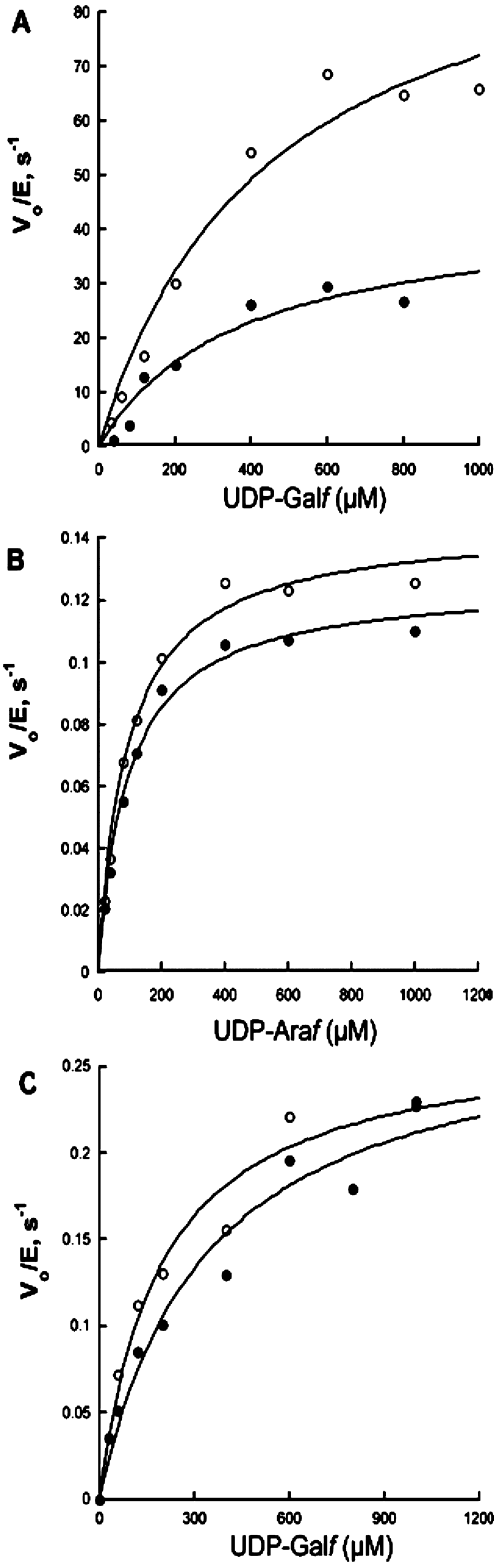

Figure 1. Activities of *Af*UGM and W315A with UDP-Gal*f* or UDP-Ara*f* as the substrate. (A) Wild-type *Af*UGM with UDP-Gal*f* as the substrate. (B) Wild-type *Af*UGM with UDP-Ara*f* as the substrate. (C) W315A single mutant with UDP-Gal*f* as the substrate. Empty circles correspond to assays performed in H_2O and filled circles those in D_2O.

in the RLS of the reaction.[37] The results are expressed as $^{D_2O}k_{cat}$, the ratio of k_{cat} measured in H_2O to that measured in D_2O.

The KSIE was measured for wild-type *Af*UGM and W315A. Using wild-type *Af*UGM with UDP-Gal*f*, a $^{D_2O}k_{cat}$ close to 2 was obtained, consistent with proton exchange being part of the RLS. In contrast, a $^{D_2O}k_{cat}$ close to 1 was obtained with the wild-type enzyme and UDP-Ara*f*, indicating that a proton transfer is not part of the RLS. Similarly, a $^{D_2O}k_{cat}$ of ∼1 was obtained using W315A and UDP-Gal*f* (Figure 1 and Table 1). Thus, the KSIE of W315A with the natural substrate is similar to that of wild-type *Af*UGM with UDP-Ara*f*.

Kinetic Solvent Viscosity Effects. KSVE experiments were performed to determine if product release contributes to the RLS. The ratio of k_{cat} in water $[(k_{cat})_o]$ to k_{cat} in a glycerol-containing solution $[(k_{cat})_\eta]$ was plotted as a function of the relative viscosity of the solution. The slope of this plot provides an indication of the degree to which diffusion out of the active site limits k_{cat}. Using wild-type *Af*UGM and UDP-Gal*f*, a KSVE slope of 0.25 was obtained, indicating that product release does not contribute substantially to the RLS (Figure S4 and Table 1). This result is consistent with the one obtained for the same reaction but catalyzed by *Tc*UGM.[7] In contrast, a strong dependence of the k_{cat} value on solution viscosity was observed when UDP-Ara*f* was used as the substrate with the wild-type enzyme. In this case, the slope increased to a value close to 1 (Table 1). Similarly, with W315A, the slope with either substrate was 0.8−0.9 (Figure S4 and Table 1). These results suggest that product release contributes to the RLS of both the wild-type enzyme with UDP-Ara*f* and W315A with either substrate. Thus, similar to the KSIE measurements, the KSVE of W315A with the natural substrate is similar to that of wild-type *Af*UGM with UDP-Ara*f*.

Molecular Dynamics Simulations of the Michaelis Complexes. Altogether, the kinetic data suggested that perturbing the enzyme either by using a non-natural substrate or by mutating Trp315 to Ala changed the RLS from a chemical step to product release. Classical MD simulations were performed on the *Af*UGM/UDP-Gal*p* and *Af*UGM/UDP-Ara*p* Michaelis complexes to understand how perturbation of the natural substrate impacts the active site behavior. The focus of this analysis was to investigate differential aspects between the systems, which could provide insight into the observed differential rate of product release.

A first clear difference that was noticed by visually analyzing the trajectories was the distinct position of the sugar moiety in *Af*UGM/UDP-Ara*p* with reference to the *Af*UGM/UDP-Gal*p* Michaelis complex. In *Af*UGM/UDP-Gal*p*, the O6 hydroxyl group of Gal*p* occupies a region between the benzo group of FADH and the Trp315 wall (Figure 2A). In the *Af*UGM/UDP-Ara*p* Michaelis complex, the absence of the -CH_2-OH group at C5 in Ara*p* allows a rotation of the sugar ring, which, in turn, moves it farther from the benzo ring of the FADH cofactor, generating an empty space in the active site (Figure 2B).

Noticing the void in the active site in the *Af*UGM/UDP-Ara*p* simulation, we analyzed the diffusion of water into the active site. Thus, we counted the number of water molecules within 6 Å of the $N5_{FADH}$ atom of the cofactor in all the snapshots of the MD trajectories. In Figure 3, we present the distributions of the number of water molecules in the active site for the two cases. On average, the *Af*UGM/UDP-Gal*p* Michaelis complex has six water molecules around the substrate, while the *Af*UGM/UDP-Ara*p* complex has 9−11 water molecules in the active site. This result is consistent with the lack of a -CH_2-OH group at C5 in Ara*p*.

DOI: 10.1021/acs.biochem.8b00323
Biochemistry 2018, 57, 3713−3721

Table 1. Kinetic Parameters for *Af*UGM and W315A Using UDP-Gal*f* or UDP-Ara*f* as the Substrate[a]

	*Af*UGM		W315A	
	UDP-Gal*f*	UDP-Ara*f*	UDP-Gal*f*	UDP-Ara*f*
k_{cat} (s^{-1})	100 ± 15	0.14 ± 0.005	0.27 ± 0.02	0.23 ± 0.05
K_M (μM)	450 ± 150	94 ± 11	193 ± 40	700 ± 200
k_{cat}/K_M (M^{-1} s^{-1})	230000 ± 10000	1540 ± 150	1400 ± 200	331 ± 46
$^{D_2O}k_{cat}$[b]	2.30 ± 0.25	1.16 ± 0.04	1.05 ± 0.14	not determined
KSVE slope[c]	0.25 ± 0.01	1.17 ± 0.10	0.80 ± 0.10	0.90 ± 0.06

[a]All the reactions were performed in 25 mM HEPES, 125 mM NaCl, and 20 mM dithionite (pH 7.0). [b]Kinetic solvent isotope effects were calculated by dividing the k_{cat} value determined in H_2O by the k_{cat} value measured in 90% D_2O at pD 7.0. [c]Kinetic solvent viscosity effect obtained with glycerol as the viscogen at 0.5, 10, 20, and 30%.

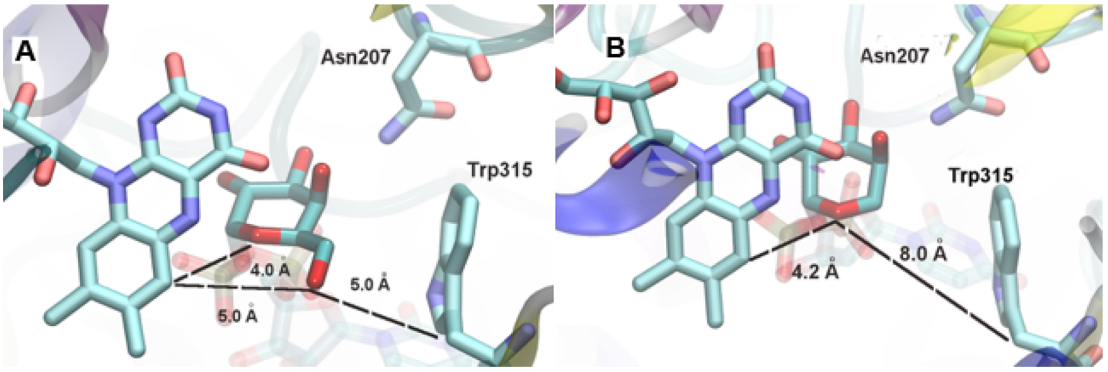

Figure 2. Binding modes of substrates in the active site of *Af*UGM. The structures shown are the most representative active site conformations from the MD simulations: (A) *Af*UGM with UDP-Gal*p* and (B) *Af*UGM with UDP-Ara*p*. The substrate, Asn207, Trp315 (or Ala315), and the isoalloxazine ring of the FADH cofactor are highlighted. Distinct characteristic distances are also indicated.

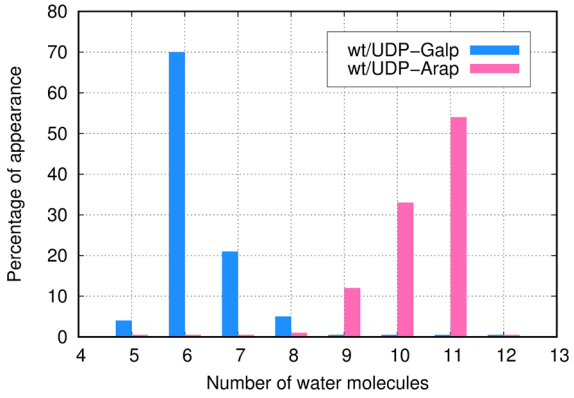

Figure 3. Distribution of the number of water molecules within 6 Å of $N5_{FADH}$ computed from the MD simulations.

Umbrella Sampling Calculations of the Chemical Rate Determinant Step. Quantum-classical MD simulations were performed to compare the free energy profiles and the conformational changes in the ring closure step of the Gal*p*–Gal*f* and Ara*p*–Ara*f* isomerizations catalyzed by *Af*UGM. Experimental and theoretical studies are consistent in indicating that after substrate binding a covalent bond is formed between the sugar moiety of the substrate and the FADH cofactor (d → e in Scheme 2), followed by the sugar ring opening process (e → f → g in Scheme 2).[7,9,18,25,28] After that, the linear form of the sugar closes into its furanose form (g → h in Scheme 2). Both computational studies and kinetic analyses of the catalytic mechanism of *Tc*UGM have identified this cyclization process as the chemical RLS of the mechanism.[7,28,33] In the current analysis, this cyclization process was also determined to be the one that presents the highest free energy barrier for the chemical steps in each case (data not shown). Therefore, we focused the analysis on this step (g → h in Scheme 2).

The free energy profiles for the ring closure step are presented in Figure 4. The calculated free energy barrier related to the Gal*p*–Gal*f* conversion catalyzed by *Af*UGM was 23 ± 1 kcal/mol. Also, a significant increase in the free energy exists at the beginning of the process (from a value of approximately −5.0 to approximately −3.0 of the reaction coordinate), which is not observed in the simulation of the Ara*p*–Ara*f* conversion (Figure 4). During this period of the reaction, there are

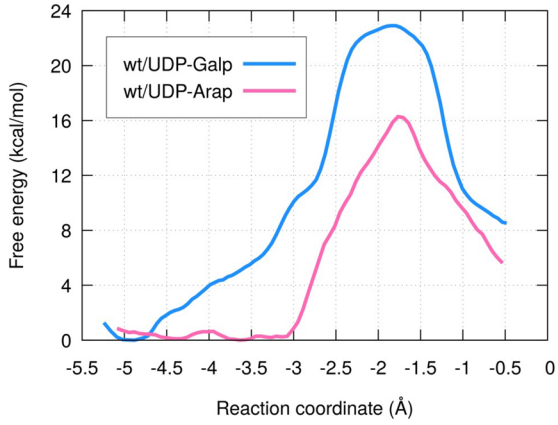

Figure 4. Free energy profiles for the ring contraction step in the catalytic mechanism of *Af*UGM. The highest barrier (23 ± 1 kcal/mol) is observed for the wild-type form of the enzyme catalyzing Gal*p*–Gal*f* conversion (blue line). For the Ara*p*–Ara*f* isomerization catalyzed by *Af*UGM (pink line), the barrier is significantly smaller. Movies available as Supporting Information depict these simulations.

DOI: 10.1021/acs.biochem.8b00323
Biochemistry 2018, 57, 3713–3721

concerted changes in the orientation of the sugar hydroxyl groups before any bond is broken or formed. While $O4_{GAL}$ approaches $C1_{GAL}$, torsional changes around the C−C bonds caused the $O5_{GAL}$ and $O6_{GAL}$ hydroxyl groups to move away from $C1_{GAL}$. These conformational rearrangements appear to be restrained by the presence of Trp315. Movie S1 depicts the conformational changes mentioned above.

With regard to the cyclization step for the Ara*p*−Ara*f* conversion catalyzed by *Af*UGM, the calculated barrier was 16 ± 1 kcal/mol, which is ∼30% lower than that obtained with the native substrate (Figure 4). Unlike the Gal*p*−Gal*f* conversion, the initial reorientation of the sugar group has almost no energy cost (Figure 4, pink line). This can be explained considering that, as the $O6_{GAL}$ group is not present in arabinose, its restrained movement is avoided and its absence facilitates the conformational rearrangements of the $O4_{GAL}$ and $O5_{GAL}$ hydroxyl groups that are needed to form the five-membered ring. Movie S2 describes these movements in this case.

DISCUSSION

Enzymatic reaction mechanisms can be divided into three parts: Michaelis complex formation, chemical reaction, and product release. Any of these stages can contribute to the RLS of the catalytic cycle.[29,38,39] For the Gal*p*−Gal*f* tautomerization catalyzed by UGM, it has been shown that ring cyclization controls the overall rate of the catalytic cycle.[7] In this work, we studied how the RLS switches from a chemical reaction to product release either by changing the substrate or by replacing an active site residue in the mutase reaction catalyzed by *Af*UGM. In particular, we first measured the activity of *Af*UGM catalyzing either the Gal*p*−Gal*f* or Ara*p*−Ara*f* conversion and that of the W315A single mutant catalyzing the Gal*p*−Gal*f* isomerization. Then, to better understand the difference in the activities, kinetic solvent viscosity and kinetic solvent isotopic experiments with classical and quantum-classical molecular dynamics simulations were performed.

For the Gal*p*−Gal*f* conversion catalyzed by *Af*UGM, a KSIE value of ∼2 suggested that a slow proton transfer step is the main RLS, while the KSVE results indicated that product release is only partially rate limiting. We assigned the rate-limiting solvent sensitive step to the ring contraction step (g → h in Scheme 2). This is supported by the umbrella sampling free energy calculations, which showed that the estimated barrier for this sugar contraction step is 23 ± 1 kcal/mol. This barrier was the highest obtained for the cases studied and is consistent with the values found for the same step in the Gal*p*−Gal*f* isomerization catalyzed by *Tc*UGM.[28] Analysis of the conformational changes that occur during this cyclization process indicated that, at the beginning of this reaction and prior to any bond breaking/formation event, the torsional rearrangements around the C−C bonds of the sugar that orient $O4_{GAL}$, $O5_{GAL}$, and $O6_{GAL}$ hydroxyl groups are restrained by the presence of the Trp315 wall. In addition, when the atomic details of the Michaelis complex were investigated by classical MD simulations, it was observed that only a small number of water molecules are present in the active site.

The Gal*p*−Gal*f* conversion catalyzed in the absence of the Trp wall in W315A occurred with a k_{cat} value that was several hundred-fold lower than for *Af*UGM. KSIE results for W315A indicate that there are no protons in flight in the RLS, in contrast to what was observed with *Af*UGM. Furthermore, the KSVE results suggest that product release is significantly more rate-limiting than the same reaction catalyzed by the wild-type form. A possible explanation is that the extra space afforded by the absence of the Trp315 wall lowers the free energy barrier of the cyclization step of the catalytic mechanism, allowing product release to become rate-limiting.

For Ara*p*−Ara*f* isomerization catalyzed by *Af*UGM, it was found that the k_{cat} was 0.14 ± 0.005 s^{-1}, which is significantly lower than that for the Gal*p*−Gal*f* conversion. However, it is similar to the k_{cat} value for Gal*p*−Gal*f* isomerization catalyzed by W315A. In this case, KSIE results also indicate that the ring contraction step is not rate-limiting and KSVE results confirm that product release is the rate determinant step. Thus, the experimental results revealed that for *Af*UGM, both the substitution of the substrate Gal*p* for Ara*p* and the replacement of Trp315 with Ala cause the same effect, a decrease in the turnover number and a switch in the rate-limiting step from ring contraction to product release. The computed free energy barrier for the sugar contraction process for Ara*p*−Ara*f* conversion was ∼30% lower than that of the Gal*p*−Gal*f* conversion catalyzed by wild-type *Af*UGM. This lower energy value for the Ara*p*−Ara*f* conversion is supported by the lack of a KSIE. For this case, it could also be observed that the reorientation of hydroxyl groups of the sugar that are needed during the initial period of the cyclization process takes place with no energy cost. We attribute this to the absence of the $-CH_2-OH$ substituent; thus, the rearrangement of the other sugar hydroxyl groups is not hindered. Classical MD simulations of this system showed that there are almost twice as many water molecules in the active site. This fact could have a detrimental effect on the rate of product release. Together, the data presented here provide further insight into the roles of the Trp wall in the reaction of UGM and of steric control in enzyme catalysis.

ASSOCIATED CONTENT

Supporting Information

The Supporting Information is available free of charge on the ACS Publications website at DOI: 10.1021/acs.biochem.8b00323.

Figures describing the chemical mechanism, the spectra of *Af*UGM with both UDP and UDP-Ara*f*, the alignment of eukaryotic UGMs, and solvent viscosity effect results (PDF)

Movie related to the conformational rearrangements of the sugar moiety at the beginning of the ring closure step observed in the WT/UDP-Gal*p* simulations (AVI)

Movie related to the conformational rearrangements of the sugar moiety at the beginning of the ring closure step observed in the WT/UDP-Ara*p* simulations (AVI)

AUTHOR INFORMATION

Corresponding Authors

*Department of Biochemistry, Virginia Tech, Blacksburg, VA 24061. E-mail: psobrado@vt.edu. Phone: (540) 231-9485. Fax: (540) 231-9070.

*Department of Biochemistry, University of Missouri—Columbia, Columbia, MO 65211. E-mail: tannerjj@missouri.edu. Phone: (573) 884-1280.

ORCID

John J. Tanner: 0000-0001-8314-113X

Pablo Sobrado: 0000-0003-1494-5382

DOI: 10.1021/acs.biochem.8b00323
Biochemistry 2018, 57, 3713−3721

Author Contributions

P.S., G.P.-S., and J.J.T. designed the study. P.S., G.P.-S., R.C.-P., and J.J.T. wrote the paper. I.D.F. and K.K. purified UGM and performed mutagenesis and characterization. I.D.F. performed the KSVE and KSIE experiments. P.S., K.K., J.J.T., G.P.-S., and R.C.-P. conceived and designed the calculations. G.P.-S., R.C.-P., I.D.F., K.K., J.J.T., and P.S. discussed the results.

Funding

Research reported in this publication was supported by National Institute of General Medical Sciences (NIGMS) Grant R01GM094469, National Science Foundation Grant CHE-1506206, and PICT 2436 préstamo BID. The authors are also very grateful to CONICET for financial support.

Notes

The authors declare no competing financial interest.

■ ABBREVIATIONS

Gal*p*, galactopyranose; Gal*f*, galactofuranose; Ara*p*, arabinopyranose; Ara*f*, arabinofuranose; UGM, UDP-galactopyranose mutase; RLS, rate-limiting step; *Af*UGM, *A. fumigatus* UDP-galactopyranose mutase; *Tc*UGM, *T. cruzi* UDP-galactopyranose mutase; KSVE, kinetic solvent viscosity effect; KSIE, kinetic solvent isotope effect; PDB, Protein Data Bank; MD, molecular dynamics; US, umbrella sampling.

■ REFERENCES

(1) Beverley, S. M., Owens, K. L., Showalter, M., Griffith, C. L., Doering, T. L., Jones, V. C., and McNeil, M. R. (2005) Eukaryotic UDP-galactopyranose mutase (GLF gene) in microbial and metazoal pathogens. *Eukaryotic Cell 4*, 1147−1154.

(2) Latge, J. P. (2009) Galactofuranose containing molecules in Aspergillus fumigatus. *Med. Mycol. 47* (Suppl.1), S104−S109.

(3) Richards, M. R., and Lowary, T. L. (2009) Chemistry and biology of galactofuranose-containing polysaccharides. *ChemBioChem 10*, 1920−1938.

(4) Nassau, P. M., Martin, S. L., Brown, R. E., Weston, A., Monsey, D., McNeil, M. R., and Duncan, K. (1996) Galactofuranose biosynthesis in Escherichia coli K-12: identification and cloning of UDP-galactopyranose mutase. *J. Bacteriol. 178*, 1047−1052.

(5) Trejo, A. G., Haddock, J. W., Chittenden, G. J., and Baddiley, J. (1971) The biosynthesis of galactofuranosyl residues in galactocarolose. *Biochem. J. 122*, 49−57.

(6) Barlow, J. N., Girvin, M. E., and Blanchard, J. S. (1999) Positional Isotope Exchange Catalyzed by UDP-Galactopyranose Mutase. *J. Am. Chem. Soc. 121*, 6968−6969.

(7) Oppenheimer, M., Valenciano, A. L., Kizjakina, K., Qi, J., and Sobrado, P. (2012) Chemical mechanism of UDP-galactopyranose mutase from Trypanosoma cruzi: a potential drug target against Chagas' disease. *PLoS One 7*, e32918.

(8) Soltero-Higgin, M., Carlson, E. E., Gruber, T. D., and Kiessling, L. L. (2004) A unique catalytic mechanism for UDP-galactopyranose mutase. *Nat. Struct. Mol. Biol. 11*, 539−543.

(9) Sun, H. G., Ruszczycky, M. W., Chang, W. C., Thibodeaux, C. J., and Liu, H. W. (2012) Nucleophilic participation of reduced flavin coenzyme in mechanism of UDP-galactopyranose mutase. *J. Biol. Chem. 287*, 4602−4608.

(10) Tanner, J. J., Boechi, L., Andrew McCammon, J., and Sobrado, P. (2014) Structure, mechanism, and dynamics of UDP-galactopyranose mutase. *Arch. Biochem. Biophys. 544*, 128−141.

(11) Oppenheimer, M., Poulin, M. B., Lowary, T. L., Helm, R. F., and Sobrado, P. (2010) Characterization of recombinant UDP-galactopyranose mutase from Aspergillus fumigatus. *Arch. Biochem. Biophys. 502*, 31−38.

(12) Dhatwalia, R., Singh, H., Solano, L. M., Oppenheimer, M., Robinson, R. M., Ellerbrock, J. F., Sobrado, P., and Tanner, J. J. (2012) Identification of the NAD(P)H binding site of eukaryotic UDP-galactopyranose mutase. *J. Am. Chem. Soc. 134*, 18132−18138.

(13) Dhatwalia, R., Singh, H., Oppenheimer, M., Karr, D. B., Nix, J. C., Sobrado, P., and Tanner, J. J. (2012) Crystal structures and small-angle x-ray scattering analysis of UDP-galactopyranose mutase from the pathogenic fungus Aspergillus fumigatus. *J. Biol. Chem. 287*, 9041−9051.

(14) van Straaten, K. E., Routier, F. H., and Sanders, D. A. (2012) Structural insight into the unique substrate binding mechanism and flavin redox state of UDP-galactopyranose mutase from Aspergillus fumigatus. *J. Biol. Chem. 287*, 10780−10790.

(15) Dhatwalia, R., Singh, H., Oppenheimer, M., Sobrado, P., and Tanner, J. J. (2012) Crystal structures of Trypanosoma cruzi UDP-galactopyranose mutase implicate flexibility of the histidine loop in enzyme activation. *Biochemistry 51*, 4968−4979.

(16) Beis, K., Srikannathasan, V., Liu, H., Fullerton, S. W., Bamford, V. A., Sanders, D. A., Whitfield, C., McNeil, M. R., and Naismith, J. H. (2005) Crystal structures of Mycobacteria tuberculosis and Klebsiella pneumoniae UDP-galactopyranose mutase in the oxidised state and Klebsiella pneumoniae UDP-galactopyranose mutase in the (active) reduced state. *J. Mol. Biol. 348*, 971−982.

(17) Gruber, T. D., Borrok, M. J., Westler, W. M., Forest, K. T., and Kiessling, L. L. (2009) Ligand binding and substrate discrimination by UDP-galactopyranose mutase. *J. Mol. Biol. 391*, 327−340.

(18) Gruber, T. D., Westler, W. M., Kiessling, L. L., and Forest, K. T. (2009) X-ray Crystallography Reveals a Reduced Substrate Complex of UDP-Galactopyranose Mutase Poised for Covalent Catalysis by Flavin. *Biochemistry 48*, 9171−9173.

(19) Partha, S. K., Sadeghi-Khomami, A., Slowski, K., Kotake, T., Thomas, N. R., Jakeman, D. L., and Sanders, D. A. (2010) Chemoenzymatic synthesis, inhibition studies, and X-ray crystallographic analysis of the phosphono analog of UDP-Galp as an inhibitor and mechanistic probe for UDP-galactopyranose mutase. *J. Mol. Biol. 403*, 578−590.

(20) Karunan Partha, S., van Straaten, K. E., and Sanders, D. A. (2009) Structural basis of substrate binding to UDP-galactopyranose mutase: crystal structures in the reduced and oxidized state complexed with UDP-galactopyranose and UDP. *J. Mol. Biol. 394*, 864−877.

(21) Poulin, M. B., Shi, Y., Protsko, C., Dalrymple, S. A., Sanders, D. A. R., Pinto, B. M., and Lowary, T. L. (2014) Specificity of a UDP-GalNAc Pyranose−Furanose Mutase: A Potential Therapeutic Target for Campylobacter jejuni Infections. *ChemBioChem 15*, 47−56.

(22) Sanders, D. A., Staines, A. G., McMahon, S. A., McNeil, M. R., Whitfield, C., and Naismith, J. H. (2001) UDP-galactopyranose mutase has a novel structure and mechanism. *Nat. Struct. Biol. 8*, 858−863.

(23) van Straaten, K. E., Kuttiyatveetil, J. R. A., Sevrain, C. M., Villaume, S. A., Jiménez-Barbero, J., Linclau, B., Vincent, S. P., and Sanders, D. A. R. (2015) Structural Basis of Ligand Binding to UDP-Galactopyranose Mutase from Mycobacterium tuberculosis Using Substrate and Tetrafluorinated Substrate Analogues. *J. Am. Chem. Soc. 137*, 1230−1244.

(24) Wangkanont, K., Winton, V. J., Forest, K. T., and Kiessling, L. L. (2017) Conformational Control of UDP-Galactopyranose Mutase Inhibition. *Biochemistry 56*, 3983−3992.

(25) Mehra-Chaudhary, R., Dai, Y., Sobrado, P., and Tanner, J. J. (2016) In Crystallo Capture of a Covalent Intermediate in the UDP-Galactopyranose Mutase Reaction. *Biochemistry 55*, 833−836.

(26) Da Fonseca, I., Qureshi, I. A., Mehra-Chaudhary, R., Kizjakina, K., Tanner, J. J., and Sobrado, P. (2014) Contributions of unique active site residues of eukaryotic UDP-galactopyranose mutases to substrate recognition and active site dynamics. *Biochemistry 53*, 7794−7804.

(27) Lide, D. (2000) *Handbook of Chemistry and Physics 2000−2001*, CRC Press, Boca Raton, FL.

(28) Pierdominici-Sottile, G., Cossio Perez, R., Galindo, J. F., and Palma, J. (2014) QM/MM molecular dynamics study of the galactopyranose –> galactofuranose reaction catalysed by Trypanosoma cruzi UDP-galactopyranose mutase. *PLoS One 9*, e109559.

DOI: 10.1021/acs.biochem.8b00323
Biochemistry 2018, 57, 3713−3721

(29) Pierdominici-Sottile, G., Horenstein, N. A., and Roitberg, A. E. (2011) Free Energy Study of the Catalytic Mechanism of Trypanosoma cruzitrans-Sialidase. From the Michaelis Complex to the Covalent Intermediate. *Biochemistry 50*, 10150−10158.
(30) Pierdominici-Sottile, G., and Roitberg, A. E. (2011) Proton Transfer Facilitated by Ligand Binding. An Energetic Analysis of the Catalytic Mechanism of Trypanosoma cruzi Trans-Sialidase. *Biochemistry 50*, 836−842.
(31) Woodcock, H. L., Hodošček, M., and Brooks, B. R. (2007) Exploring SCC-DFTB Paths for Mapping QM/MM Reaction Mechanisms. *J. Phys. Chem. A 111*, 5720−5728.
(32) Barnett, C. B., and Naidoo, K. J. (2010) Ring Puckering: A Metric for Evaluating the Accuracy of AM1, PM3, PM3CARB-1, and SCC-DFTB Carbohydrate QM/MM Simulations. *J. Phys. Chem. B 114*, 17142−17154.
(33) Huang, W., and Gauld, J. W. (2012) Tautomerization in the UDP-galactopyranose mutase mechanism: a DFT-cluster and QM/MM investigation. *J. Phys. Chem. B 116*, 14040−14050.
(34) Kumar, S., Rosenberg, J. M., Bouzida, D., Swendsen, R. H., and Kollman, P. A. (1992) THE weighted histogram analysis method for free-energy calculations on biomolecules. I. The method. *J. Comput. Chem. 13*, 1011−1021.
(35) Rosta, E., and Hummer, G. (2015) Free Energies from Dynamic Weighted Histogram Analysis Using Unbiased Markov State Model. *J. Chem. Theory Comput. 11*, 276−285.
(36) Zhang, Q., and Liu, H. W. (2001) Chemical synthesis of UDP-beta-L-arabinofuranose and its turnover to UDP-beta-L-arabinopyranose by UDP-galactopyranose mutase. *Bioorg. Med. Chem. Lett. 11*, 145−149.
(37) Northrop, D. B. (1982) [30] Deuterium and tritium kinetic isotope effects on initial rates. In *Methods in Enzymology* (Purich, D. L., Ed.) pp 607−625, Academic Press.
(38) Callender, R., and Dyer, R. B. (2015) The Dynamical Nature of Enzymatic Catalysis. *Acc. Chem. Res. 48*, 407−413.
(39) Shannon, A. E., Pedroso, M. M., Chappell, K. J., Watterson, D., Liebscher, S., Kok, W. M., Fairlie, D. P., Schenk, G., and Young, P. R. (2016) Product release is rate-limiting for catalytic processing by the Dengue virus protease. *Sci. Rep. 6*, 37539.

DOI: 10.1021/acs.biochem.8b00323
Biochemistry 2018, 57, 3713−3721